CENTRE FOR ELECTRON MICROSCOPY AND MICROANALYSIS (CEMM)

The Centre for Electron Microscopy and Microanalysis (CEMM) is an instrumental centre at the JSI that comprises analytical equipment in the field of electron microscopy and microanalysis. Access to the research equipment of the CEMM is enabled to other JSI departments as well as other research institutions, universities and industrial partners. The equipment at the CEMM is used by researchers, interested in the morphology and structural and chemical characterization of materials between the micrometre and the atomic level. Part of the centre was completely renovated and reorganized in 2020. The reason for the renovation was optimization of environment due to the purchase of two new scanning electron microscopes and to provide better working conditions for the microscopes' users and employees (Figures 1 and 2). At the CEMM there are currently installed three scanning electron microscopes (SEM) JSM-7600F, Verios G4 HP and Quanta 650, two transmission electron microscopes (TEM) JEM-2100 (CO NiN) and JEM-2010F, and the equipment for the TEM and SEM sample preparation. Additionally, the IJS is a co-owner (20%) of a JEM-ARM200CF (transmission electron microscope with atomic resolution) at the Chemical Institute.

Figure 1. Centre for Electron Microscopy and Microanalysis (CEMM).

Figure 2. Renovated room for the JSM-7600F microscope.

In 2020, we began training operators on the new state-of-the-art Verios G4 HP high-resolution scanning electron microscope, Thermo Fisher Scientific (Figure 3). The microscope is the only one of its kind in this part of Europe and provides extremely high resolution at low excitation voltages. It also features automatic pattern insertion, the ability to observe non-conductive patterns, and exceptional Z-contrast even at low voltages. In addition to the highly sensitive EDXS detector, the microscope is equipped with a transmission detector (STEM) as well.

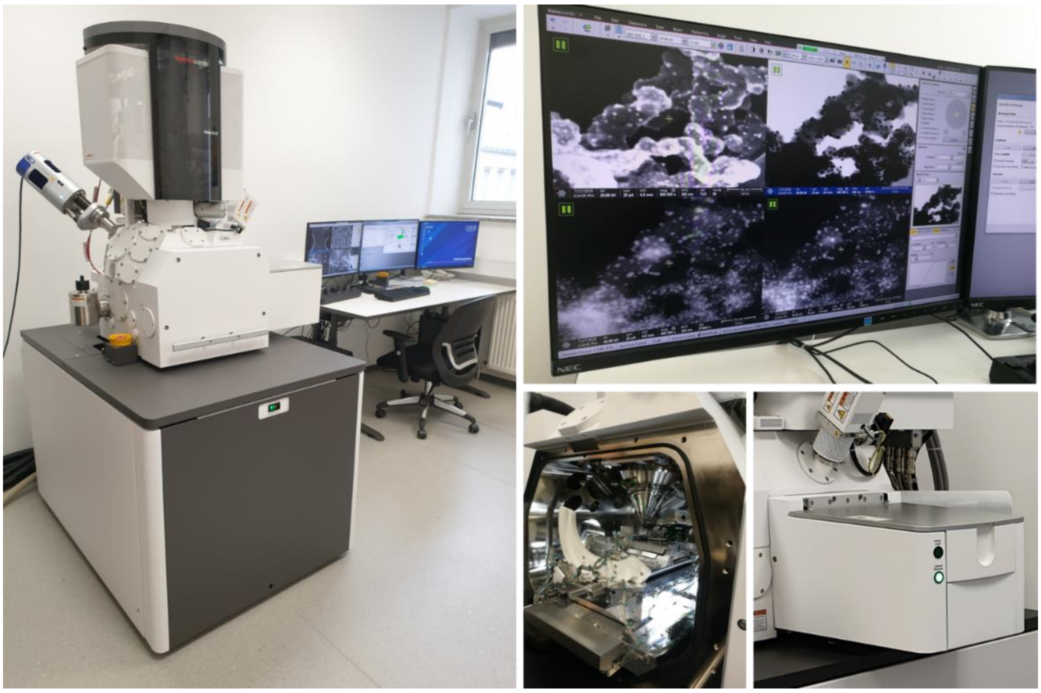

Figure 3. Verios 4G HP microscope.

We also started training operators in 2020 on the new Quanta 650 electron microscope, Thermo Fisher Scientific (Figure 4). The main feature of this microscope is that it is operational in three vacuum ranges that are achieved through differential pumping. This allows us to investigate a wide range of materials, both conductive and non-conductive.

Figure 4. ESEM Quanta 650 microscope.

The research involving the equipment at the CEMM is diverse and du to many different materials and the use of different analytical techniques.

- Scanning electron microscopy is employed to observe the morphology and structure of the surfaces and for the microstructural investigation and determination of the chemical composition. Samples that are mostly investigated are ceramics (polycrystalline oxide and non-oxide compositions), nanostructured materials, metallic magnetic materials, metals, alloys glass, etc. All of the scanning electron microscopes in the CEMM are equipped with an energy-dispersion (EDXS) and / or wavelength dispersion (WDXS) spectrometer for X-rays, allowing non-destructive determination of the chemical composition of the investigated materials. The scanning electron microscope JSM-7600F is additionally equipped with an electron back-scattered diffraction (EBSD) detector and an electron lithography system. The equipment of the Verios 4G HP microscope enables the observation of the morphology of nanoparticles and samples extremely sensitive to electron doses and the observation of transmission samples (STEM). The Quanta 650 microscope allows the observation of larger, conductive or non-conductive samples.
- Transmission electron microscopy (TEM) provides an insight into the structure of the material on the nano-scale (atomic level). Transmission electron microscopy enables structural and chemical analyses of the grain boundaries and study of precipitates, planar defect and dislocation determination. Additionally, to ceramic samples also other materials and structures are investigated such as thin films

on different substrates, alloys, delicate metallic magnetic materials, polymers, etc. Transmission electron microscope JEM-2100 is equipped with an EDXS spectrometer and a CCD camera, and the JEM-2010F is additionally equipped with a scanning transmission electron (STEM) unit, EDXS and EELS (electron energy loss) spectrometers, and a CCD camera.

- The CEMM also manages the necessary equipment for the SEM and TEM sample preparation.

The operation of the Centre is managed by properly trained employees. Besides maintenance of the equipment, other CEMM activities include, among other, training of new operators, organization of workshops and conferences on the topic of electron microscopy, providing services for industrial partners and implementation of new analytical techniques. CEMM personnel are also responsible for the dissemination of electron microscopy techniques to the general public in the scope of organized visits to the IJS, as well through publications in traditional and digital media.

Examples of microstructural and nanostructural investigations using the CEMM equipment

The examples of analyses of structural and chemical characterisations of different materials using electron microscopy techniques were performed by the CEMM employees as well as operators from different JSI departments.

1. Polypropylene membrane analysis

A study of sterilization of polypropylene membranes in previously ionized face masks was performed. (Figure 5).

In: Pirker. L.; Pogačnik Kranjc. A.; Malec. J.; Radulović. V.; Gradišek. A.; Jelen. A.; Remškar. M.; Mekjavić. I.B.; Kovač. J.; Miran. M.; Snoj. L. Sterilization of polypropylene membranes of facepiece respirators by ionizing radiation. Journal of membrane science, 2021, 619, 118756

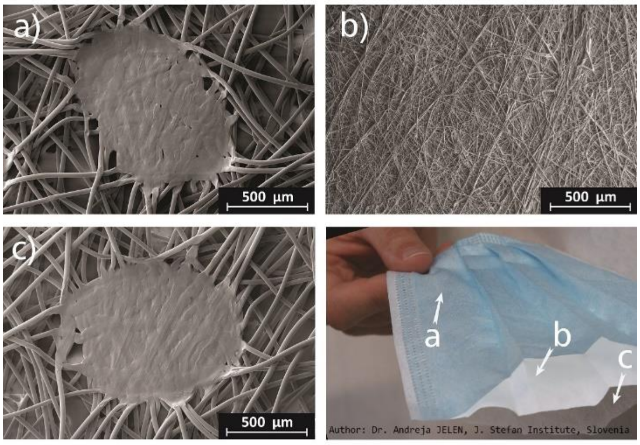

Figure 5. SEM image of polypropylene membrane (Jelen A., F5, JSM-7600F)

2. $CaCO_3$ aragonite analysis

SEM analysis of samples from water dispenser showed the presence of $CaCO_3$ aragonite crystals (Figure 6).

Figure 6. SEM image of $CaCO_3$ aragonite crystals (Samardzija Z., K7, Verios 4G HP).

3. NdFeB magnet

NdFeB magnet analysis showed preferential grain orientation. The grains are below 1 micrometer in size (Figure 7).

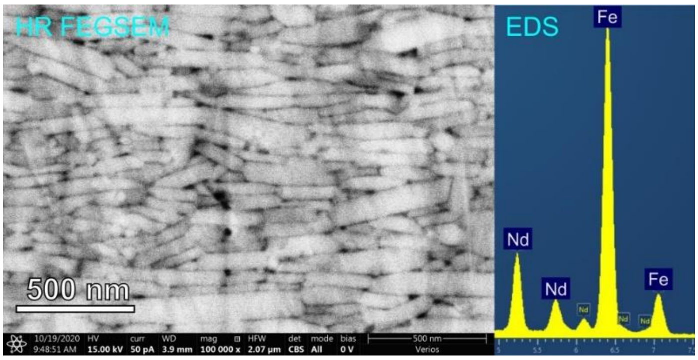

Figure 7. High resolution BSE image and EDS analysis of NdFeB magnet (Samardzija Z., K7, Verios 4G HP).

4. Granulate

Internal structure of ZnO-based granules. The image was taken without spattering of the sample (Figure 8).

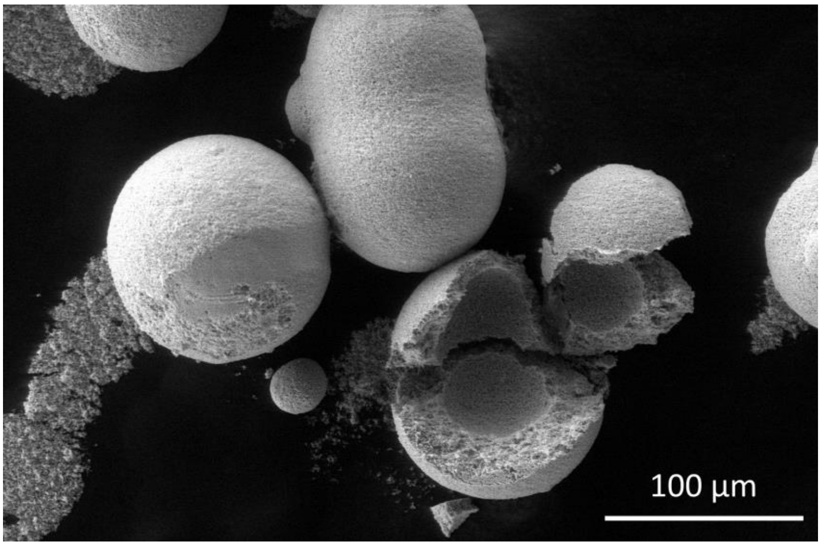

Figure 8. SEM image of granulate under a low vaccum conditions (Bernik S., K7, Koblar M, CEMM, Quanta 650).

5. Microplastics- fibers

Images of polymer fibers within the study of microplastic degradation (Figure 9).

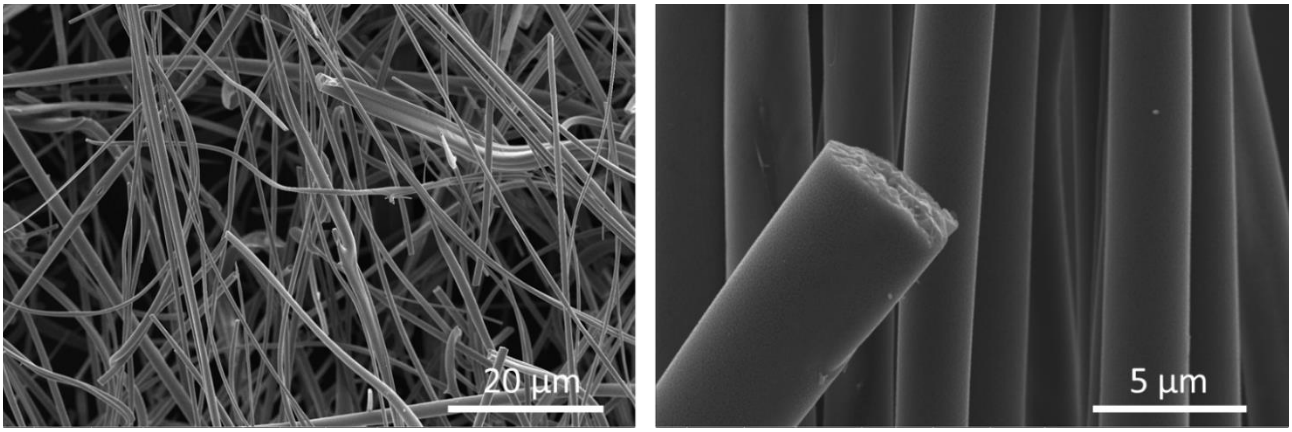

Figure 9. SEM image of fibers (Radoševič T., K9, Koblar M, CEMM, Quanta 650).

6. WO_3 nanowires with IrO_2 particles

An SEM and TEM study of WO_3 nanoparticles coated with IrO_2 nanoparticles was performed, according to different synthetic procedures and according to different concentrations of crystalline IrO_2 nanoparticles on WO_3 nanoparticles (Figure 10).

In: Navarrete. E.; Bittencourt. C.; Umek. P.; Cossement. D.; Guell. F.; Llobet. E. Tungsten trioxide nanowires decorated with iridium oxide nanoparticles as gas sensing material. Journal of alloys and compounds, 2020, 812, 152156-1-152156-9

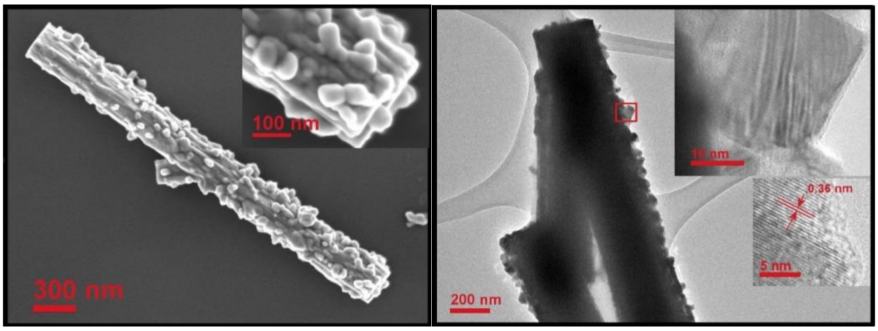

Figure 10. SEM and TEM image of WO_3 nanowires with IrO_2 nanoparticles (Umek P., F5, JEM-2100).

7. A study of the effect of TiO_2 nanoparticle properties on pneumonia

As part of the investigation of the influence of the physical and chemical properties of nanoparticles on pneumonia, TEM analyzes of TiO_2 nanoparticles and nanotubes, nanocuboids and quartz were performed (Figure 11).

In: Danielsen. P.; Štrancar. J.; Umek. P.; Koklič. T.; Garvas. M.; et al. Effects of physicochemical properties of TiO_2 nanomaterials for pulmonary inflammation, acute phase response and alveolar proteinosis in intratracheally exposed mice. Toxicology and applied pharmacology, 2020, 386, 114830-1-114830-18

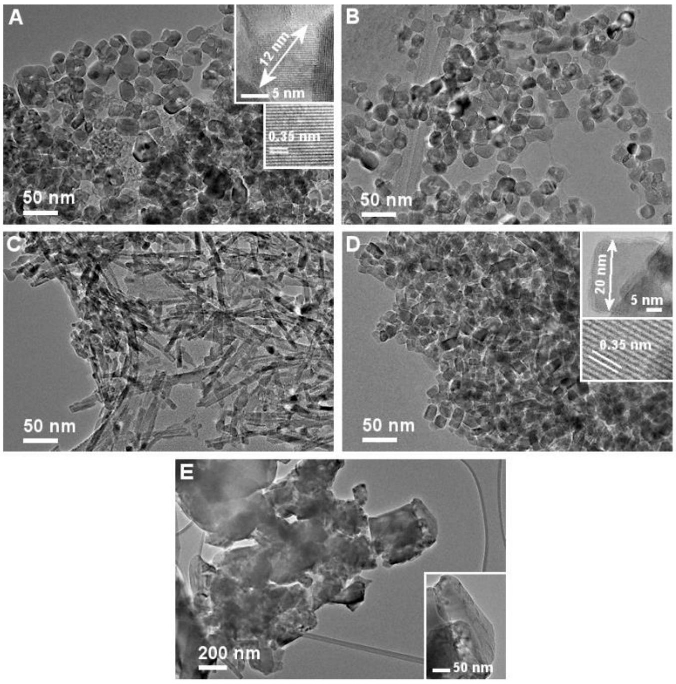

Figure 11. TEM images of commercial TiO_2 samples (A, B) on the laboratory scale of synthesized TiO_2 nanotubes and nanocubides (C, D) and commercial quartz sample DQ12 (Umek P., F5, JEM-2100).

8. TEM study of Zn-Al hydroxide

TEM study of the morphological characteristics of layered Zn-Al hydroxide with Mo-doped TiO_2 nanoparticles in the interlayer space used in catalytic processes (Figure 12).

In: Cerc Korošec. R.; Miljević. B.; Umek. P.; Bergh. J. M. van der.; Vučetić. S.; Ranogajec. J. Photocatalytic self-cleaning properties of Mo:TiO_2 loaded Zn-Al layered double hydroxide synthesised at optimised pH value for the application on mineral substrates. Ceramics international, 2020, 46, 6756-6766

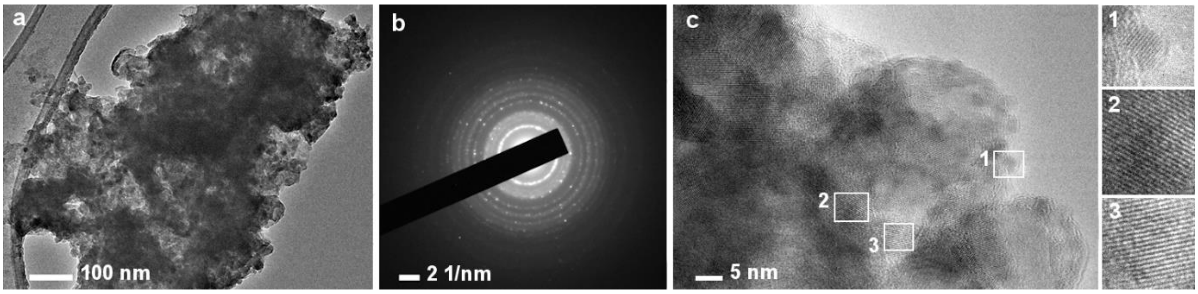

Figure 12. TEM study of layered Zn-Al hydoxide with Mo-doped TiO_2 nanoparticles (Umek P., F5, JEM-2100).

9. TEM study of TiON nanotubes

In TEM, a study of TiON nanotubes inside which Ir grains were trapped was performed. TiON analysis helped to complete a study of the effect of metallic Ir within TiON nanotubes on increasing the efficiency of catalytic reactions (Figure 13).

In: Bele. M.; Jovanovič. P.; Marinko. Ž.; Drev. S.; Šelih. V. S.; Kovač. J.; Gaberščček. M.; Koderman Podboršek. G.; Dražić. G.; Hodnik. N.; Kokalj. A.; Suhadolnik. L. Increasing the oxygen-evolution reaction performance of nanotubular titanium oxynitride-supported Ir nanoparticles by a strong metal-support interaction. ACS Catalysis, 2020, 10, 13688-13700

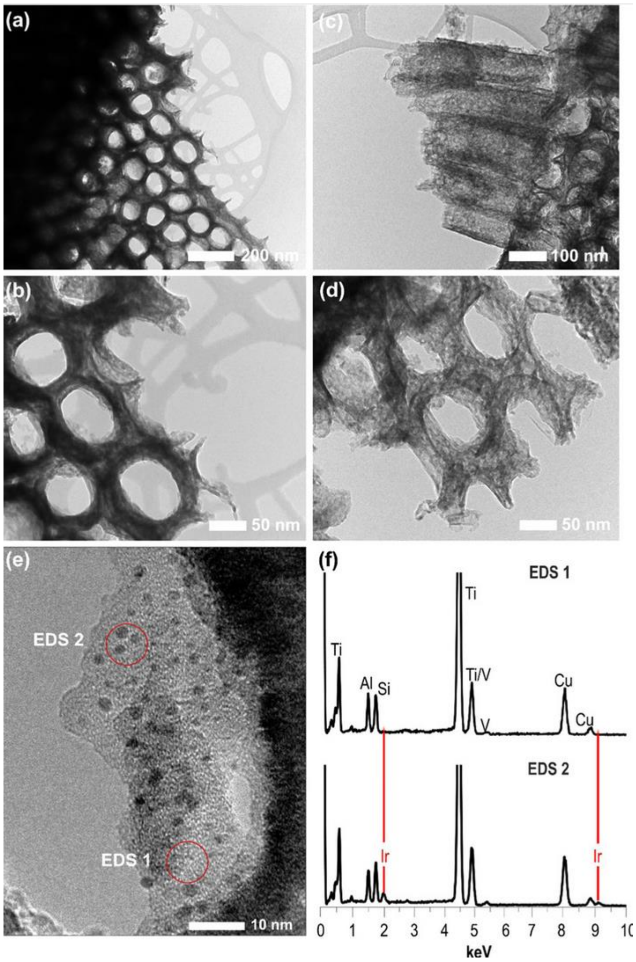

Figure 13. TEM images of TiON nanotubes: (a, b, d) top view and (c) side view of nanotubes. (e) TEM image of TiON nanotubes with Ir nanoparticles (f) and accompanying EDS analysis (Drev S., CEMM, JEM-2010F).

10. Adsorption of zinc on the surface of a carbon nanotube

TEM study of the position of zinc atoms and clusters of atoms absorbed on the surface of a carbon nanotube. HAADF and BF STEM analysis were performed (Figure 14).

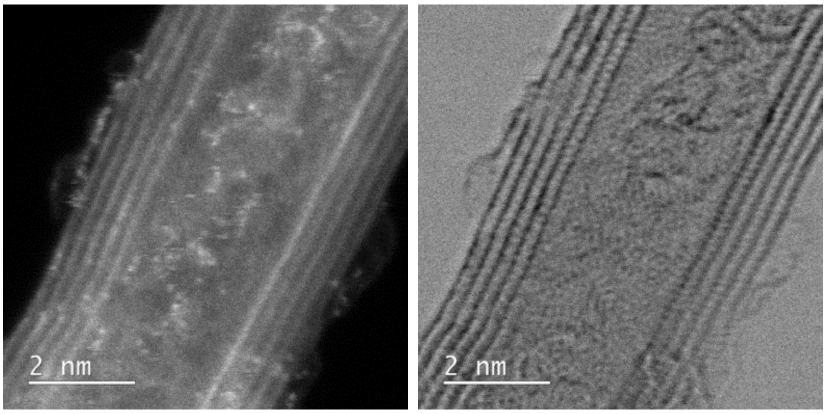

Figure 14. HAADF and BF STEM images of zinc atoms and clusters of atoms on the carbon nanotube (Makovec D., K8, JEM-ARM200F).

11. Defects in $BiFeO_3$ domain walls

High-angle annular dark-field (HAADF) STEM images of DWs (a,c) with corresponding normalized distribution maps of Bi-column intensities before (b) and after the application of the electric field (d), respectively. These regions correspond to the areas marked with full orange boxes in panels (a,c). Insets in panels (a,c) show the Fe displacement directions (relative to the Bi sublattice) in the two adjacent domains, with dashed-yellow boxes indicating DW regions. The reduction of the Bi-atom column intensities within the DW in pristine sample (b) indicates the presence of Bi vacancies. In contrast, no evidence of Bi-vacancy accumulation at newly formed DW (d) was found after application of an electric field (Figure 15).

In: Benčan. A.; Dražić. G.; Uršič Nemevšek. H.; Komelj. M.; Rojac. T. Domain-wall pinning and defect ordering in $BiFeO_3$ probed on the atomic and nanoscale. Nature communication, 2020, 11, 1762-1-1762-8

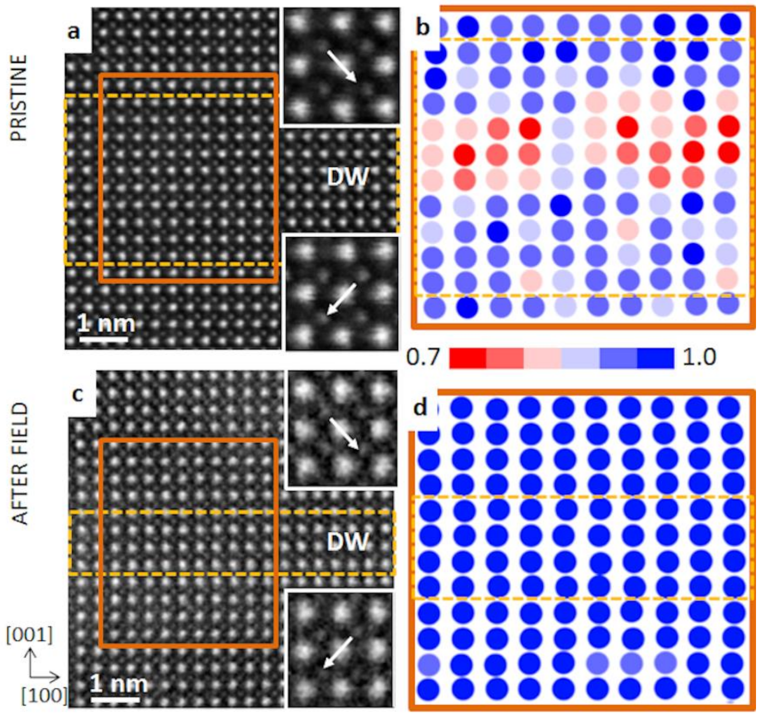

Figure 15. HAADF STEM images of domain wall in $BiFeO_3$ (Bencan A., Dražić G., K5, KI, JEM-ARM200F).

12. High precision determination of ZnO interface using DFT and HRTEM

High precision determination of interface structures using *ab-initio* calculations (DFT) and high-resolution transmission electron microscopy (HRTEM). Two inversion boundary (IB) structures in Sb_2O_3-doped ZnO: (**a**) the reported one (Rečnik *et al*. 2001), based on single stacking fault, and (**b**) the new, more stable one, as predicted by DFT screening, that is based on a double stacking fault sublattice (Ribić *et al*. 2020). Combination of experimental and computational approaches allows determination of fine structural details with confidence levels down to <1 pm. The study is a result of collaboration between the Institute for Multidisciplinary Research in Belgrade and Jožef Stefan Institute in Ljubljana. Experimental work was conducted at the CEMM in Ljubljana (Figure 16).

In: Ribić. V.; Rečnik. A.; Komelj. M.; Kokalj. A.; Branković. Z.; Zlatović. M.; Branković. G.; New inversion boundary structure in Sb-doped ZnO predicted by DFT calculations and confirmed by experimental HRTEM. Acta Materialia, 2020, 199, 633-648

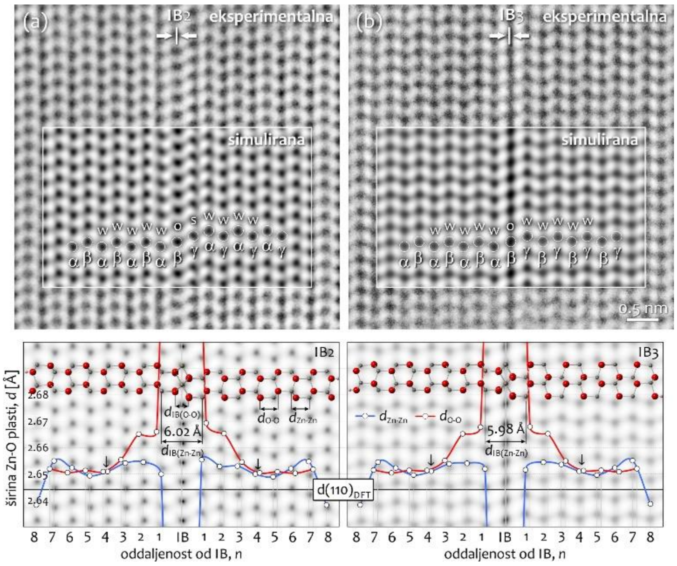

*Figure 16. Two inversion boundary (IB) structures in Sb_2O_3-doped ZnO: (**a**) the reported one (Rečnik et al. 2001), based on single stacking fault, and (**b**) the new, more stable one, as predicted by DFT screening, that is based on a double stacking fault sublattice (Ribić et al. 2020). (Rečnik A., Ribić V., K7, JEM-2010F).*

13. High precision determination of ZnO interface using DFT and HRTEM

A study of the growth and possible effects of voltage on ferroelectric domains in epitaxial heterostructures was performed (Figure 17 and 18).

In: Belhadi, J.; Gabor, U.; Uršič, H.; Daneu, N.; Kim, J.; Tian, Z.; Koster, G.; Martin, LW.; Spreitzer, M. Growth mode and strain effect on relaxor ferroelectric domain in epitaxial 0.67Pb(Mg1/3Nd2/3)O3-0.33PbTiO3/SrRuO3 heterostructures. RSC Adv., 2021, 11, 1222-1232

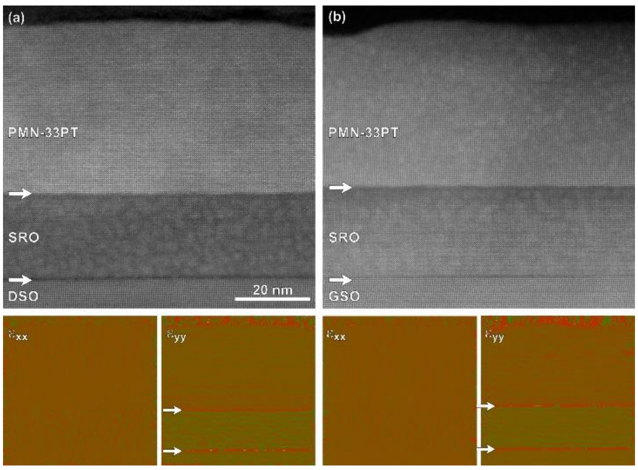

Figure 17. HAADF-STEM cross-section images of $0.67Pb(Mg_{1/3}Nb_{2/3})O_3/SrRuO_3/DyScO_3$ (a) and $0.67Pb(Mg_{1/3}Nb_{2/3})O_3/SrRuO_3/GdScO_3$ (b) heterostructures and their corresponding GPA analysis of the in-plane (ε_{xx}) and out-of-plane (ε_{yy}) lattice strains (Daneu N, K9, JEM-ARM200F).

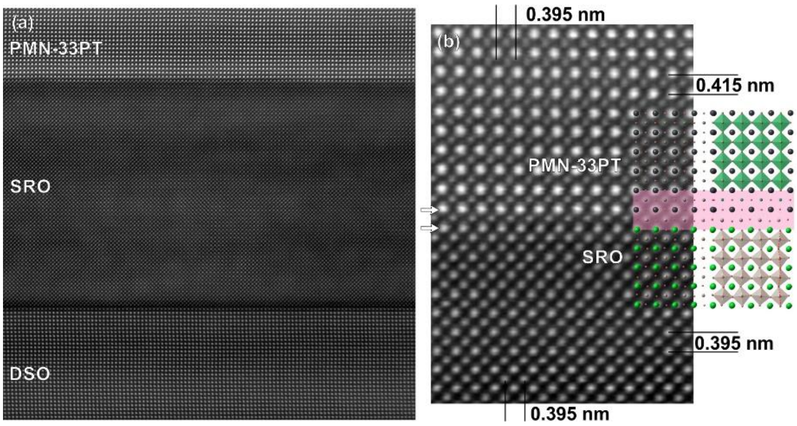

Figure 18. (a) Filtered HAADF-STEM image of the 0.67Pb($Mg_{1/3}Nb_{2/3}$)O_3/$SrRuO_3$/$DyScO_3$ heterostructure showing a continuous transition of atomic columns from the substrate across the two interfaces without the presence of dislocations. The DSO–SRO contact is sharp and follows single atomic layer, whereas the SRO/PMN-33PT heterointerface makes steps to neighboring atomic planes (atomic mixing at the A-sites and B-sites is likely). (b) Local atomic structure of the SRO/PMN–33PT heterointerface, where the SRO layer ends with the B-site layer (RuO_2) and the PMN–33PT layer starts with the A-site layer (PbO). Tilting of RuO_6 and perhaps also the (($Mg_{2/9}Nb_{4/9}Ti_{3/9}$)O_6) octahedra directly at the contact is likely (pink region) (Daneu N, K9, JEM-ARM200F).

EMPLOYEES

1. **Prof. Miran Čeh, head**
2. Dr. Sandra Drev
3. Dr. Jitka Hreščak
4. Andreja Šestan Zavašnik, dipl. Inž. Kem. Inž.
5. Maja Koblar, univ. dipl. fiz.